A first-principles study of phase transitions in ultrathin films of BaTiO$_3$

J PAUL[1], T NISHIMATSU[2,3], Y KAWAZOE[2] and U V WAGHMARE[1,*]

[1]Theoretical Sciences Unit, Jawaharlal Nehru Centre for Advanced Scientific Research, Jakkur, Bangalore 560 064, India
[2]Institute for Materials Research, Tohoku University, Sendai 980-8577, Japan
[3]Rutgers University, 136 Frelinghuysen Road, Piscataway, NJ 08544-8019, USA
*Corresponding author. E-mail: waghmare@jncasr.ac.in

Abstract. We determine the effects of film thickness, epitaxial strain and the nature of electrodes on ferroelectric phase transitions in ultrathin films of BaTiO$_3$ using a first-principles effective Hamiltonian in classical molecular dynamics simulations. We present results for polarization and dielectric properties as a function of temperature and epitaxial strain, leading to size-dependent temperature–strain phase diagram for the films sandwiched between 'perfect' electrodes. In the presence of non-vanishing depolarization fields when non-ideal electrodes are used, we show that a stable stripe-domain phase is obtained at low temperatures. The electrostatic images in the presence of electrodes and their interaction with local dipoles in the film explain these observed phenomena.

1. Introduction

Materials which are spontaneously polarized below a certain temperature and the direction of polarization is switchable by an external electric field, are called ferro-electrics [1]. Properties of these materials in low-dimensional systems are found to be extremely sensitive to electrical as well as mechanical boundary conditions [2,3]. Such nano-dimensional systems form essentially important components which are used in micro- as well as nano-electromechanical systems and in the fabrication of ferroelectric random access memories (FERAMS). In the case of ferroelectric (FE) thin films, electrodes and the substrate, also an electrode, on which the film is grown determine the boundary conditions and these cause the behavior of thin films to be exceptionally different from bulk. It was shown by Choi *et al* [4], that epitaxial strain imposed by substrate can be efficiently used to tune and enhance FE properties of BaTiO$_3$ films.

Spontaneous polarization in thin films along the z-direction (perpendicular to the film plane) accumulates bound charges at the film surface producing depolarization

fields which in turn cause suppression of polarization in this direction. Sandwiching the film between electrodes whose free charges partially compensate the bound surface charges, can stabilize ferroelectricity down to thicknesses of 6 and 3 unit cells [5,6]. It was recently demonstrated by Paul *et al* [7], that the presence of electrodes produces thickness dependence of FE transitions even when the depolarization fields vanish. Such a spectacular observation is essentially due to the interaction between images of local dipoles in the film and their electrostatic images in the electrodes, and it is the in-plane components that produce this effect.

In this paper, we present results of molecular dynamics simulations using an effective Hamiltonian [8,9] for BaTiO$_3$ along with a simple model for electrodes. We report (i) the dependence of polarization and dielectric properties on temperature and epitaxial strain and (ii) temperature–epitaxial strain phase diagram for films of varying thicknesses, both (i) and (ii) in the presence of vanishing depolarization fields (ideal electrodes). In the presence of non-vanishing depolarization fields (non-ideal electrodes), we report formation of stripe-like domains in the (0 1 0) planes which prevail even at high temperatures.

2. Method

2.1 *Effective Hamiltonian*

It has been confirmed by both experiments and theoretical calculations that ferroelectric transitions in BTO involve only very small structural distortions of the cubic perovskite structure. These distortions can be described in terms of the 15 normal modes (12 optical and 3 acoustic phonons) per unit cell. However, out of these 15 modes, only three acoustic modes (corresponding to inhomogeneous strain) and three lowest energy transverse optical phonon modes or the 'soft modes' (corresponding to polarization) are found to contribute significantly to these transitions. Anharmonicity in polarization (up to fourth order), elastic, electrostrictive, short-range and long-range dipolar interactions are all included in this effective Hamiltonian. Parameters of H_{eff} used in our simulations are the ones determined in refs [8,9] with density functional theory calculations using local density approximation. This results in the underestimation of the lattice constant of BaTiO$_3$. This has been compensated by performing all simulations with a negative pressure of -5 GPa.

2.2 *Model for electrodes*

We have used a simple electrostatic model for electrodes as described in ref. [10]. The two electrodes are placed on either side of the film at a distance $d/2$ from the film surface. This 'gap' (or dead layer) produces a finite depolarization field within the thin film given by [10]

$$E_{\text{d}} = -4\pi \frac{d}{l+d} P_z \hat{z}, \tag{1}$$
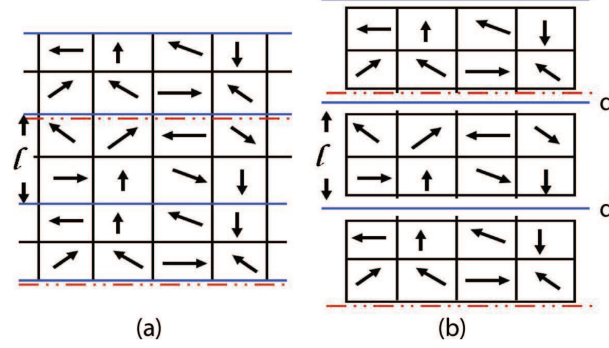
Figure 1. Schematic representation of (**a**) perfect and (**b**) imperfect electrodes sandwiching a FE thin film of thickness l. The thick red dotted lines bound the periodic box of our simulations and the lines in blue represent the electrodes. Each arrow represents the dipole moment of the supercell. At a distance $d/2$ an electrode is placed on either side of the film in (**b**).

where P_z is the out-of-plane polarization in the film and l is the thickness of film (l and d are in units of number of unit cells). For $d = 0$, we get $E_{\rm d} = 0$, which corresponds to the case of 'perfect' electrodes. The case for non-vanishing depolarization field within the film is treated with $d = 1$, and this case is referred to as 'imperfect' electrodes. Using identical electrodes on either side of the film allows us to simulate our systems using periodic boundary conditions since the electrodes act as two mirrors producing infinite number of images (see figure 1). Due to this, the periodic box becomes twice as large as the supercell ($2(l + d)$, l and d in units of number of unit cells), i.e., we simulate our systems using doubly periodic boundary conditions. Within the electrode, the dipole is the electrostatic image of the corresponding dipole in the thin film. The out-of-plane component of the image–dipole points in the same direction as that of the dipole in the film, but the in-plane components point in opposite directions. The magnitudes of the original and image dipoles remain unaltered. We have studied two types of films sandwiched between perfect and imperfect electrodes: (a) bulk-like films which have no epitaxial constraint (system F) and (b) films whose in-plane strain degree of freedom is fixed (by the substrate on which it is grown; here it is the electrodes), referred to as epitaxial thin films (system EF). Pure bulk simulations without 'mirror'-boundary conditions are also performed for comparison with film results.

2.3 *Molecular dynamics simulations*

We used a mixed-space molecular dynamics scheme developed in refs [11,12]. Calculations of short- and long-range interactions are performed in real and in Fourier spaces respectively, which effectively reduce the computational time from $O(N^2)$ to $O(N \log N)$ where N is the system size ($N = L_x L_y L_z$). This allows us to simulate systems of larger dimensions (system sizes of $16 \times 16 \times l$ with $l = 2$ to 11 have been simulated). The efficacy of the simplectic Nosè-Poincarè [13] thermostat, which is
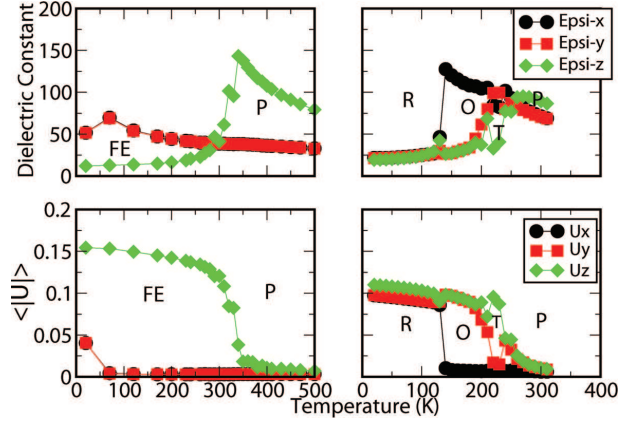
Figure 2. The top and bottom figures display dielectric constant and polarization ($P = U \times Z^*/V$: U is the displacement (in Å), Z^* is the Born-effective charge (in Coulomb), and V is the volume of one unit cell), respectively, as a function of temperature, for (left panel) epitaxial and (right panel) bulk-like thin film of thickness 4 unit cell layers placed between perfect electrodes. Left panel: P denotes high temperature paraelectric phase and FE denotes low temperature ferroelectric phase. Right panel: P, T, O and R denote paraelectric, tetragonal, orthorhombic and rhombohedral phases respectively.

implemented in our code, allows us to use a large timestep of 2 fs. The systems are thermalized for initial 30,000 timesteps and then averaged for 70,000 timesteps. To evaluate and reduce the effects of hysteresis, we use heating and cooling simulations, where the temperature was increased and decreased in steps of 20 K and 10 K, away from and near the transition region, respectively.

3. Results and discussion

3.1 *Perfect electrodes*

We first discuss results obtained when films (both F and EF) are placed between perfect electrodes ($d = 0$). We have already reported in ref. [7] the thickness dependence of transition temperatures with and without epitaxial constraints. We find that the transition temperatures of the bulk-like films (system F) converge to bulk behavior with increasing film thickness (see figure 2 of ref. [7]). In the presence of epitaxial strain, only one transition is observed to low-temperature tetragonal phase and the transition temperature is much higher when compared to its bulk counterpart. The in-plane degrees of freedom are fixed by the introduction of epitaxial constraint and hence the xy-transition temperatures remain almost unchanged at 70 K $\pm$ 10 K with film thickness variation. For both bulk-like and epitaxial films (systems F and EF), the high temperature paraelectric phase was found to have tetragonal symmetry, the tetragonality being more pronounced for the EF systems (see figure 2) (epitaxy favors uniaxiality, hence enhancing the tetragonality). The
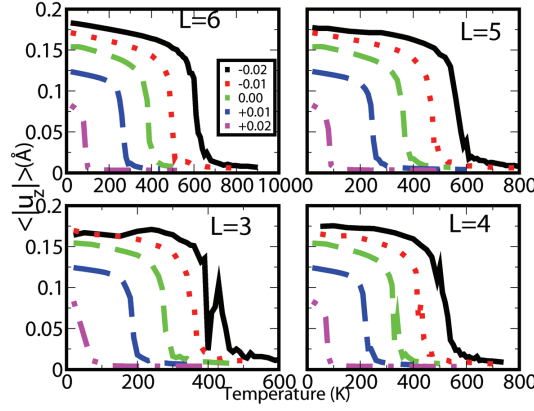
Figure 3. Polarization ($P = u_z \times Z^*/V$) as a function of temperature for epitaxial films of thicknesses $l = 3$, 4, 5 and 6 unit cells at epitaxial strain values from -0.02 to $+0.02$.

presence of electrodes breaks the horizontal reflection symmetry since the images of in-plane components of the dipole moments have opposite direction. It is the interaction of these image dipoles with those in the film that results in the thickness dependence of transition temperature which is so different from the bulk.

The variation in polarization as a function of temperature (P–T) (see figure 3) is almost independent of the film thickness since all four panels show roughly the same nature of variation. For a film of given thickness the transition temperature increases as the strain changes from tensile to compressive. For compressive strains below $\epsilon < 0.01$ there is only one transition to a phase with tetragonal structure. When strains become tensile, transitions to states with in-plane polarization is also observed. The plots also show that polarization values at low temperatures increase with strain from $+0.02$ to -0.02.

We present temperature–epitaxial strain phase diagram for films of thicknesses 3, 4, 5 and 6 unit cell layers sandwiched between perfect electrodes (figure 4). In our earlier paper [7], we presented this diagram for the epitaxial thin film of thickness 4 unit cells. The magnitude of the epitaxial strain is varied from (compressive) -0.02 to (tensile) $+0.02$ in steps of 0.01. With increasing film thickness the out-of-plane transition temperature $T_c(z)$ increases as the strain changes to compressive from tensile. At a tensile strain of 0.02, $T_c(z)$ for films of all thicknesses is 80 K (± 10 K), whereas at a compressive strain of magnitude -0.02, the temperature increases from 410 K ($l = 3$ unit cells) to 610 K ($l = 6$ unit cells). The in-plane transition temperatures increase as epitaxial strain changes from compressive to tensile and is independent of film thickness. There are four regions of this phase diagram: Region I, where a single transition to the tetragonal state occurs for strain values less than -0.005: in Region II (below 0.012) $P_x = P_y < P_z$ and in Region III (above 0.012) $P_x = P_y > P_z$; here distorted rhombohedral phase is observed and in Region IV a single transition to orthorhombic phase occurs. At strain value of 0.012, there occurs a second-order phase transition from cubic to rhombohedral phase and this is seen to be almost independent of film thickness (see inset, figure 4). Such phase
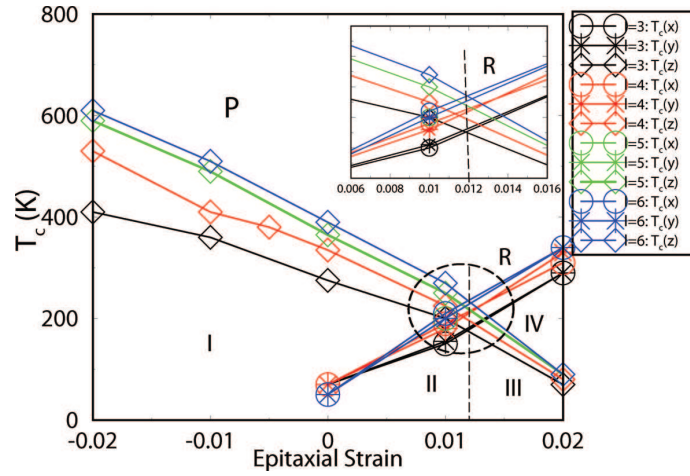
Figure 4. Temperature–strain phase diagram for films of thicknesses $l = 3$, 4, 5 and 6 unit cells placed in between perfect electrodes ($d = 0$). Region I is tetragonal, II and III are distorted rhombohedral and IV is orthorhombic. R denotes the rhombohedral phase. The inset shows that the point R occurs at almost the same value of epitaxial strain ($\sim$0.012) for films of all thicknesses.

diagrams have been studied by Diéguez *et al* [14] and Pertsev *et al* [15]. Our diagram resembles the former with two main added features that arise due to electrodes and dependence on film thickness. Firstly the point R gets shifted from 0.00 to $\sim$0.012 and secondly, the transition temperatures reduce by $\sim$70 K.

3.2 *Imperfect electrodes*

When the BaTiO$_3$ films are sandwiched between imperfect electrodes ($d = 1$), non-vanishing depolarization fields are strong and suppress the z-polarization completely, thereby producing no phase transition to state with polarization along this direction. In case of bulk-like films (F), due to the absence of epitaxy, the in-plane transition temperatures are observed to be around $\sim$210 K, whereas for epitaxial thin films, it remains constant around 70 K. We have presented here snapshots of the system at low (50 K) and high (350 K) temperatures for epitaxial thin films (figure 5). We find that at both low (50 K) as well as high (350 K) temperatures, the system shows stripe-like domains polarized along $\pm z$-axis (figures 5a, b). However, at higher temperatures the number of dipoles pointing along z-direction reduces. The in-plane (($0\,0\,1$) plane) patterns show that domains are more 'organized' at 50 K and get 'scattered' when the temperature reaches 350 K (figures 5c, d). Fong *et al* had observed similar domain patterns for PbTiO$_3$ in an X-ray synchrotron study [6].
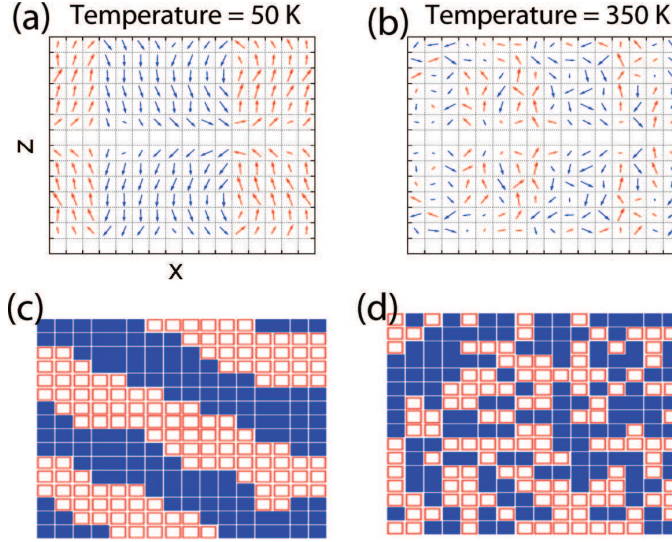
Figure 5. The stripe-like domains viewed in a $(0\,1\,0)$ plane (**a**) and (**b**), and in a $(0\,0\,1)$ plane (**c**) and (**d**) at 50 K and 350 K respectively for an epitaxial film of thickness 6 unit cell layers (strain = 0.00) sandwiched between imperfect electrodes ($d = 1$). The up-pointing and down-pointing arrows in diagrams (**a**) and (**b**), and the open and closed boxes in diagrams (**c**) and (**d**) represent $+z$ and $-z$ polarized sites.

4. Summary

To summarize, we have studied the effect of thickness as well as of the nature of electrodes on ferroelectric transition properties of ultrathin BaTiO₃ films. In the presence of perfect electrodes, we have studied these phase transitions as a function of epitaxial strain and film thicknesses, and find that the P–T behavior is almost independent of film thickness. The polarization increases as the epitaxial strain changes from tensile to compressive. The temperature–epitaxial strain phase diagram for films of thicknesses ($l = 3$, 4, 5 and 6) sandwiched between perfect electrodes shows that the out-of plane transition temperatures increase with increasing film thickness and decreases when the epitaxial strain increases (from compressive to tensile). The in-plane transition temperatures increase with strain changing from compressive to tensile for a film of given thickness. But their dependence on film thickness is seen to be much weaker compared to the out-of-plane components. In the presence of imperfect electrodes, we find that the depolarization fields suppress the out-of-plane polarization and produces stripe-like domains.

References

[1] M E Lines and A M Glass, *Principles and applications of ferroelectrics and related materials* (Oxford University Press, New York, 1977)

[2] J F Scott and C A P de Araujo, *Science* **246**, 1400 (1989)

[3] C H Ahn, K M Rabe and J M Triscone, *Science* **303**, 488 (2004)

[4] K J Choi, M Biegalski, Y L Li, A Sharan, J Schubert, R Uecker, P Reiche, Y B Chen, X Q Pan, V Gopala, L Q Chen, D G Schlom and C B Eom, *Science* **306**, 1005 (2004)

[5] J Junquera and P Ghosez, *Nature (London)* **422**, 506 (2003)

[6] D D Fong, G B Stephenson, S K Streiffer, J A Eastman, O Auciello, P H Fuoss and C Thompson, *Science* **304**, 1650 (2004)

[7] J Paul, T Nishimatsu, Y Kawazoe and U V Waghmare, *Phys. Rev. Lett.* (*in press*)

[8] W Zhong, D Vanderbilt and K M Rabe, *Phys. Rev. Lett.* **73**, 1861 (1994)

[9] W Zhong, D Vanderbilt and K M Rabe, *Phys. Rev.* **B52**, 6301 (1995)

[10] M Dawber, P Chandra, P B Littlewood and J F Scott, *J. Phys.: Condens. Matter* **15**, L393 (2003)

[11] U V Waghmare, E J Cockayne and B P Burton, *Ferroelectrics* **291**, 187 (2003)

[12] B P Burton, E J Cockayne and U V Waghmare, *Phys. Rev.* **B72**, 064113 (2005)

[13] S D Bond, B J Leimkuhler and B B Laird, *J. Comput. Phys.* **151**, 114 (1999)

[14] O Diéguez, S Tinte, A Antons, C Bungaro, J B Neaton, K M Rabe and D Vanderbilt, *Phys. Rev.* **B69**, 212101 (2004)

[15] N A Pertsev, A G Zembilgotov and A K Tagantsev, *Phys. Rev. Lett.* **80**, 1988 (1998)